Bayesian Analysis of Morphological Changes Associated with Mild Cognitive Impairment: A Cross-Sectional Study

Hanchuan Peng[*], Susan M. Resnick [‡], Dinggang Shen [†], Christos Davatzikos [†], and Edward H. Herskovits [†]

[*] NERSC Division, Lawrence Berkeley National Laboratory, MS.50F, One Cyclotron Rd, Berkeley, CA, 94720. Email: hpeng@lbl.gov

[†] Section on Biomedical Image Analysis, Department of Radiology, School of Medicine, University of Pennsylvania, 3400 Spruce Street, Philadelphia, PA, 19104. Email: herskovi@rad.upenn.edu, dgshen@rad.upenn.edu, christos@rad.upenn.edu

[‡] Laboratory of Personality and Cognition, National Institute on Aging, National Institutes of Health, Baltimore, Maryland 21224-6825. Email: resnick@lpc.grc.nia.nih.gov

ABSTRACT

In this paper we apply a new morphology-function analysis method, a Bayesian Morphometry Algorithm (BMA), to a set of cross-sectional magnetic resonance images of subjects in the Baltimore Longitudinal Study of Aging, some of whom have very mild cognitive impairment. Based on Bayesian model selection, this new method is able to test a series of hypotheses about morphology-function associations and determine morphological changes associated with clinical variables.

INTRODUCTION

The purpose of this paper is to describe the application of a new Bayesian method for morphological analysis, which can be used to determine associations among structural and clinical

variables in medical-imaging studies. We developed this algorithm because, although image data have become increasingly important to neurological clinical trials, current methods for the determination of morphology-function associations may have limited applicability. For example, in Voxel-Based Morphometry (VBM) of magnetic resonance (MR) images (Ashburner 2000; Davatzikos 2001), each voxel location is analyzed separately across all experimental cases; therefore, the number of variables equals the number of voxels (i.e., resolution elements or resels) in the image volume, which is often too large for standard statistical tests to be applied efficiently for detecting interactions among voxel and clinical variables. Multivariate methods, particularly partial least square analysis of the correlation matrix of image voxels and functional variables (e.g., experimental designs and subject behaviors) (McIntosh 1996), show promise for application to functional imaging data, and could be applied to morphological analysis as well. However, there may be cases in which nonlinear associations among brain structures and clinical variables may not be optimally modeled using this approach. In addition, the applicability of standard statistical tests, such as the t-test used in VBM, may depend on the underlying distributions of the variables, in that only the mean and standard deviation are considered in calculation of these statistics. Finally, some statistical tests may require a predefined significance threshold; in contrast, our Bayesian method requires no user input.

Recently we developed a Bayesian Morphometry Algorithm (BMA) (Peng 2001, 2002) to analyze morphology-function relationships. Given a set of morphological variables (e.g., morphological measurements) and a set of clinical variables, BMA identifies associations among sets of morphological variables and clinical variables. First, we define an *association* as probabilistic dependence among sets of morphological variables and clinical variables. Second, in BMA we compute the strength of many morphology-function associations, and select the strongest one as the *representative* association for that group of variables; this process is accomplished by Bayesian model selection (Herskovits 1991; Cooper 1992; Heckerman 1997; Buntine 1996; Glymour 1999); that is, BMA selects the most probable multivariate model of associations based on maximum a posteriori

(MAP) calculations. Third, sets of morphological variables that have similar conditional-probability distributions, given the clinical (functional) variables of interest, are consolidated into an association cluster; thus, a mechanism reflecting multivariate associations is naturally embedded in BMA. Regions of interest containing the corresponding voxels are then generated for each association cluster.

To obtain morphological variables from image data, we generate Regional Analysis of Volumes Embedded in Stereotaxic Space (RAVENS) density maps (Davatzikos 1997, 1996a, 1996b, 1998, 2001; Goldszal 1998; Shen 2001a, 2001b) from MR images of the brain, using a high-dimensional mass-preserving elastic transformation algorithm called Hierarchical Attribute Matching Mechanism for Elastic Registration (HAMMER) (Shen 2001b). The key property of the generated maps is that voxel intensity is proportional to the local volume of the corresponding brain structure prior to registration (Davatzikos 2001). Thus, voxel intensity is analogous to a volumetric measurement of the corresponding brain tissue. Since images of different subjects are put into the same stereotaxic space via registration, and volumes are preserved when generating RAVENS maps, the voxel-wise data can be compared directly, reflecting voxel-wise morphological changes of the original brain structures. Several other methods (Ashburner 2000; Friston 1995a, 1995b; Gaser 1999; Gee 1993; Thompson 1996, 1997a, 1997b; Woermann 1999) have been developed to obtain similar morphological information.

In this paper we apply BMA to cross-sectional MR image data from a sub-sample of subjects from the Baltimore Longitudinal Study of Aging (BLSA). Over the course of the BLSA, some of these individuals have developed signs of mild cognitive impairment (MCI), as defined by the Clinical Dementia Rating (CDR) scale (Morris 1993). Individuals with MCI have cognitive decline greater than expected for their age, but do not meet criteria for functional loss and dementia. MCI is associated with a high risk for conversion to Alzheimer's disease, with annual rates of conversion of 6% (Daly 2000) to 12% (Petersen 2001). Recently, Morris and colleagues have argued that 100% of individuals with MCI will develop Alzheimer's disease over 9.5 years (Morris 2001). Neuroimaging studies have

demonstrated reduced volumes of mesial temporal lobe structures, including the hippocampus and entorhinal cortex, in cross-sectional studies and accelerated rates of hippocampal volume loss in longitudinal studies (Jack 1997, 1999, 2000; Fox 1998; Xu 2000; Bobinski 1998). However, these imaging studies have focused on particular brain regions, rather than examining many structures throughout the brain. In this paper, we apply BMA to demonstrate the sensitivity of this technique to previously described volumetric changes associated with MCI, and extend these findings to other brain regions.

METHODS

In this section we first present the BMA approach, then introduce the MCI data, and related image-processing methods.

Bayesian Morphometry Algorithm

BMA is based on a Bayesian-network construction algorithm (Peng 2001, 2002; Herskovits 1991; Cooper 1992). A Bayesian Network (BN) (Jensen 1996; Glymour 1999; Heckerman 1997; Herskovits 1991; Cooper 1992; Buntine 1996) is a graphical model of probabilistic associations among a group of variables; thus, we can represent voxel-morphometric information (e. g., dilation or contraction during spatial normalization), as well as functional information (e. g., presence or absence of MCI), as variables in a BN. Directed edges in a BN model represent conditional-probability distributions among these variables. Thus, in BMA, voxel-morphological variables and clinical variables are nodes, and edges represent associations among variables. Within this framework, we have cast morphology-function analysis as the generation of a multivariate BN model from MR image data and respective clinical information.

BMA's Bayesian-network construction algorithm is based on maximum a posteriori calculations, i. e., BMA searches for the most probable Bayesian network structure given the data. In the case of

complete data for discrete variables with finite numbers of states, the formula $p(\mathbf{D}|\mathbf{S})$ for computing the probability of the data given a BN structure was first given in Herskovits (1991) and Cooper (1992), and has been called the Bayesian score for structure **S** (Cooper 1992; Heckerman 1997; Buntine 1996; Glymour 1999). Because the total number of possible BN structures (each of which is a directed acyclic graph) is super-exponential in the number of variables (Herskovits 1991), it is impossible to assess all possible structures for any nontrivial data set. Hence, we present the following method, illustrated in Fig.1, to obtain a BN structure.

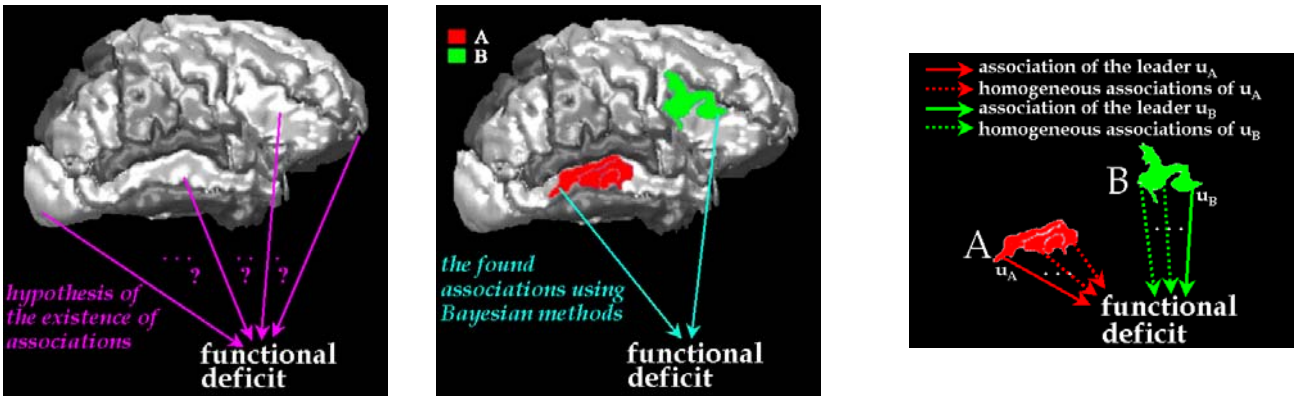

(a) Hypotheses (b) Associations generated by BMA (c) Homogeneous association regions

Fig.1 Schematic illustration of BMA: Two regions (red and green) might both be associated with a functional deficit, albeit in different ways. These regions are constructed based on identifying respective leading voxels (solid arrows), and homogeneously associated voxels (dotted arrows); these homogeneously associated voxels are often strongly associated with the leading voxels. One of the key characteristics of our approach is that it can distinguish between the red and the green regions above, based on their respective conditional-probability tables.

The overall goal of BMA, as shown in Fig.1, is to determine associations among voxel-morphological variables and clinical (functional) variables (shown as a functional deficit in Fig.1), and to consider the joint (multivariate) effect of morphological variables on the clinical variables. Initially, we have many hypotheses (one for each voxel-morphological variable) regarding associations among

voxel-morphological variables and a given clinical variable. We use the likelihood ratio computed from the Bayesian scores as measures of these hypotheses, and select the voxel-morphological variable with the largest likelihood ratio as the representative (i.e. leader) of the first group of homogeneously associated voxel variables (for details see Peng 2001, 2002). Then we use a Bayesian clustering method (Cheeseman 1995; Chickering 1997) to determine the group of voxels whose associations with the clinical variable are homogeneous, i.e., similar to the association between the first leader variable and the clinical variable. We then use the similar process, accounting for the previously detected associations, to find a second leader variable and corresponding group of homogeneously associated voxels. We repeat this process until every initial hypothesis has been tested; the resulting Bayesian network has a structure similar to those in Fig.1 (b) and (c), where there are many homogeneously associated voxels (regions A and B) represented by the leader variables u_A and u_B. The regions of interest correspond to these association clusters. (For technical details of BMA, as well as its evaluation using simulated data, see Peng (2001, 2002)).

The different association clusters have different conditional-probability distributions with respect to the clinical variable; these multivariate association patterns are not considered in commonly used statistical tests, such as the t-test. For example, in the specific case shown in Fig.1 (c), BMA has determined that the conditional-probability distribution for u_B given the clinical variable is distinct from that for u_A and the same clinical variable. Thus, the clinical variable is associated (in different ways) with both functional regions represented by u_{A} and u_{B}. In other words, BMA can reflect nonlinear associations among different regions and a clinical variable. Unlike the t-test, BMA is not based on assumptions regarding the distributions of the voxel-morphological variables, and it does not depend on a predefined significance threshold.

We described the implementation of BMA, its application to simulated data, and a comparison of its performance to that of VBM, in (Peng 2001). In the following we focus on evaluating BMA with data from the BLSA.

Application to Structural Findings Associated with MCI

As part of the BLSA neuroimaging study (Resnick 2000), MR images and clinical information are obtained annually from selected BLSA participants. The goals of this study are to determine prior physical and psychological characteristics that predict changes in brain structure and function in later life, and to determine changes in brain structure and function associated with changes in cognitive and memory performance, the rate of change in brain anatomy in normal men and women, and the frequency and progression of brain abnormalities in normal aging populations.

To demonstrate the application of BMA to cross-sectional MR data, we examined images from 40 male subjects. These subjects have varying degrees of cerebral atrophy. The MR images compared in this study consist of T1-weighted gradient-echo SPGR MR images obtained during each subject's 5th annual assessment. The size of these images is 256×256×124 voxels and the voxel resolution is 0.94mm×0.94mm×1.5mm.

Image Registration

For the purpose of this voxel-based analysis of morphological changes, we segmented gray matter (GM), white matter (WM) and cerebrospinal fluid (CSF) in each image volume using an automated technique (Goldszal 1998). Because morphological variations of CSF are implied by morphological changes of GM and WM, in this paper we examined the morphological changes of GM and WM only. We then generated RAVENS maps (Davatzikos 1997, 1996a, 1996b, 1998, 2001; Goldszal 1998; Shen 2001a, 2001b) from these segmented images. RAVENS maps are produced via a high-dimensional mass-preserving elastic transformation, which generates a number of tissue-density maps in a stereotaxic space. Mass preservation warranties that regional volumetric measurements can be performed after spatial normalization, by accounting for the amount of compression or expansion that

occurs during spatial normalization. Expansion decreases tissue density, so that the total amount of tissue remains constant, and the converse is true for compression; therefore, regional volumetric measurements are performed via regional tissue density measurements, in the stereotaxic space. For example, longitudinal atrophy would be reflected by a relative decrease of brain-tissue density in corresponding RAVENS maps over time. In this study we generated RAVENS maps with a high-dimensional elastic transformation referred to as HAMMER (Shen 2001).

After image registration, each RAVENS density map was smoothed using a Gaussian kernel to reduce registration error, as is conventional for voxel-based morphometry. For the purpose of reduction of computational burden, we down-sampled these smoothed RAVENS density maps by a factor of 2, resulting in images with size 128×128×62 voxels. In summary, this process yielded data consisting of MCI status, and GM and WM volumes for 40 subjects; 7 of these subjects had MCI; the size of each volume was 128×128×62 voxels, and the voxel resolution was 1.875mm×1.875mm×3.0mm.

Application of BMA

In our experiments, we examined associations among voxels in RAVENS maps and the MCI (functional) variable. We analyzed the GM and WM RAVENS maps separately.

Because the Bayesian score (Herskovits 1991; Cooper 1992), i. e., the scoring function for BN structures used in this paper, is defined for discrete variables, we discretized the RAVENS maps' voxel intensities. In this paper, we discretized data by thresholding the z-scores. That is, for each voxel, we calculated the mean value across subjects, and compared each case to the mean value; the assigned label was 0 when a voxel intensity was larger than or equal to the mean value, otherwise it was 1. Thus, a label '1' indicates that a subject at the corresponding voxel-location had volumetric shrinkage (i. e. atrophy), compared to the whole sample. This discretization procedure transformed the RAVENS

density maps into categorical maps, which together with the respective clinical information (MCI = "Yes" or "No"), were used as the input to BMA.

RESULTS

Subjects' ages ranged from 59 to 84 years (mean age = 69.75, standard deviation = 6.34). Of these 40 subjects, 7 were determined to have mild cognitive impairment (MCI) based on the CDR scale. The MCI subjects had mean age 72.29 and standard deviation 7.76; the non-MCI controls had mean age 69.21 and standard deviation 6.00.

In the following, we first show results obtained with the 9mm Gaussian smoothing kernel; we then show results obtained with smoothing kernels of different sizes.

In both GM and WM experiments, BMA produced two major association clusters of voxel-morphological variables with the MCI variable, from which regions of interest (ROIs) were obtained. The characteristics of these association clusters are listed in Table 1, where we represent the importance of a leader variable as $\log_e(r)$, the logarithm of the likelihood ratio of Bayesian scores with and without the corresponding edge in the BN structure. Approximately 4-5% of GM and WM voxels were found to be associated with the MCI variable. The data presented in Table 1 indicate that the strongest association is much more important than the secondary association, in that their logarithm scale factors differ substantially (6.3 vs. 4.8 and 7.0 vs. 4.4); in addition, there were relatively fewer voxels detected in the secondary association clusters (i.e. 0.45% << 3.74% and 0.58% << 4.84%). Therefore, we present only the major ROIs in the strongest association clusters. Because the model in this example did not yield multivariate associations, individual ROIs in the first association cluster obtained with BMA are visualized separately. Of note, ROIs visualized in this section represent regions with shrinkage of volume (atrophy) in the presence of MCI. Probabilities of the occurrence of MCI conditioned on atrophy of the leaders of the first association clusters (for GM and WM) are listed in Table 2, where we see that MCI is not present in the absence of atrophy in these regions, and the

probability of MCI given atrophy of the voxels in these clusters is approximately 42% for the GM cluster, and 58% for the WM cluster, respectively; note that these probabilities happen to sum to 1 by chance.

Fig.2 shows the largest ROIs found for GM. In Fig.2 (a), the first ROI returned by BMA contains disctinct (i.e., not contiguous) clusters centered on entorhinal cortex bilaterally (right more pronounced than left), and on the boundaries of the hippocampi. This result is in accordance with previously reported analyses of morphological changes associated with MCI (Jack 1997, 1999, 2000; Fox 1998; Xu 2000; Bobinski 1998; de Toledo-Morrell 2000). In Fig.2 (b), a second ROI is detected more laterally, near the inferior aspect of the left temporal lobe. Of note, accelerated longitudinal declines in lateral temporal lobe cerebral glucose metabolism have been reported in carriers for the Apolipoprotein E epsilon 4 allele, a genetic risk factor for Alzheimer's disease (Small 2000; Rapoport 2000).

Table 1. Characteristics of association clusters for examination of MCI. $\log_e(r)$ is the logarithm of the likelihood ratio for the Bayesian models with and without the corresponding association; Ω is the number of voxels in the cluster; r_Ω is the percentage of voxels in the respective tissue, i.e., GM or WM.

Association cluster #		1	2
GM	$\log_e(r)$	6.310	4.755
	Ω	7662	930
	r_Ω	3.74%	0.45%
WM	$\log_e(r)$	7.036	4.357
	Ω	9190	1108
	r_Ω	4.84%	0.58%

Table 2. Probabilities of states of the MCI variable conditioned on the states of the first leader variable found for GM and WM, respectively.

States of the first leader voxel-variable		Conditional probabilities of the MCI variable given states of the leaders	
		MCI = 'No'	MCI = 'Yes'
GM	Atrophy = 'No'	100%	0%
	Atrophy = 'Yes'	58%	42%
WM	Atrophy = 'No'	100%	0%
	Atrophy = 'Yes'	42%	58%

Fig.3 (a) and (b) show the largest ROIs found in WM association clusters; these ROIs are centered on entorhinal cortex bilaterally, consistent with the gray-matter findings presented above.

In addition to our confirmation of the associations between atrophy in mesial and lateral temporal-lobe regions and MCI, we also observed associations for GM in the left insular region, centered on the transverse temporal gyrus (Fig. 4a) and for WM centered on the inferior frontal gyrus (Fig.4b). These regions were also observed in VBM analyses of these data (for Fig.2 and Fig.3, the respective results obtained from SPM99 are shown in Fig.5 and Fig.6, respectively). For example, the largest ROIs detected by the different methods overlapped substantially, as listed in the right-most column of Table 3. Of note, each voxel represents a large region in the original non-smoothed image; anatomically, these overlapping ROIs belong to the same functional region of brain.

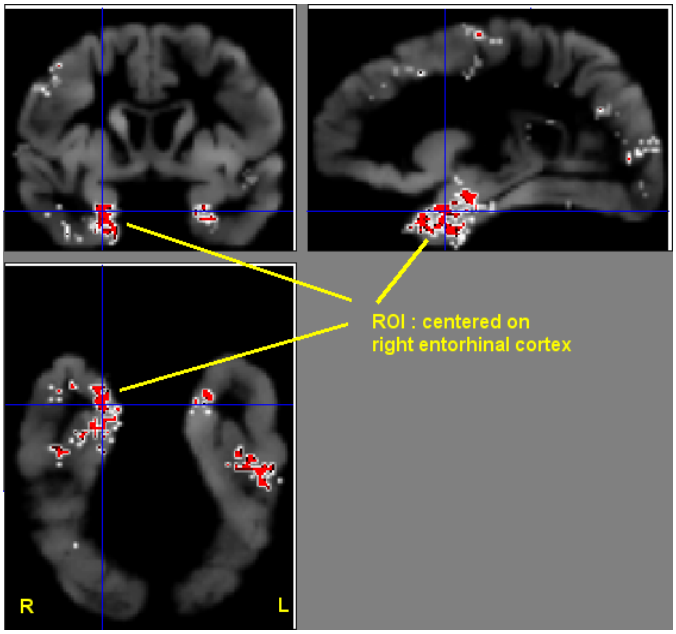

(a) ROI centered on right entorhinal cortex

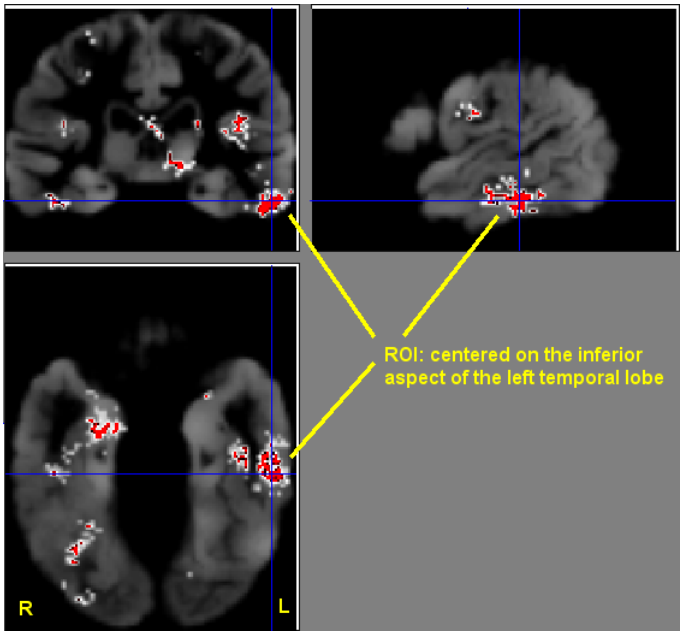

(b) ROI centered on the inferior aspect of the left temporal lobe

Fig.2 Gray-matter detection results (red) overlaid on the average RAVENS density map of all subjects' GM volumes. Regions in red depict ROIs found in the first association cluster.

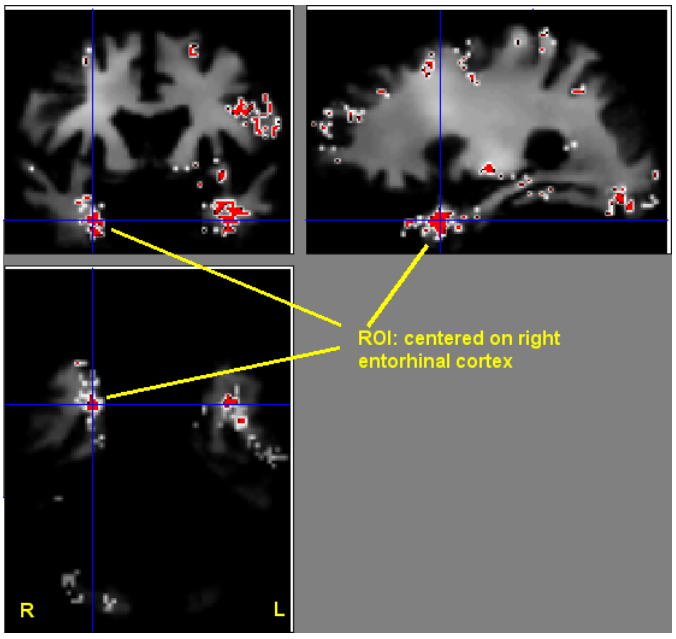

(a) ROI centered on right entorhinal cortex

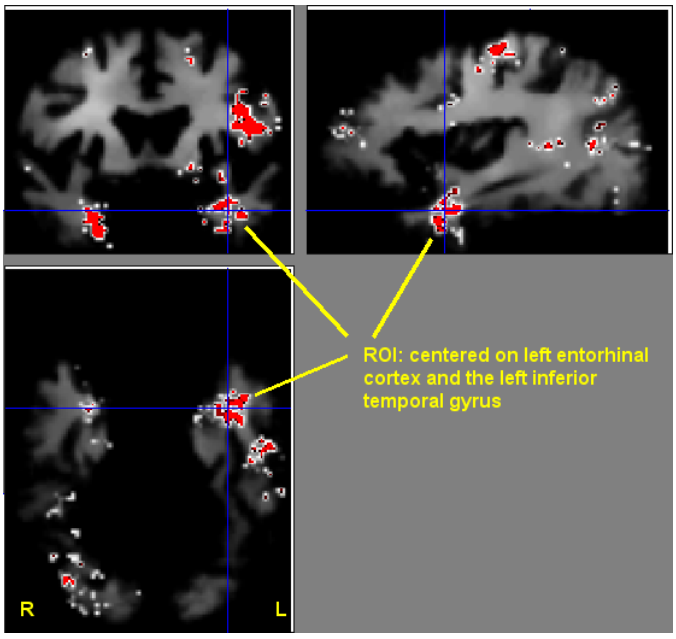

(b) ROI centered on left entorhinal cortex and the left inferior temporal gyrus

Fig.3 White-matter detection results (red) overlaid on the average RAVENS density map of all subjects' WM volumes. Red depicts ROIs found in the first association cluster.

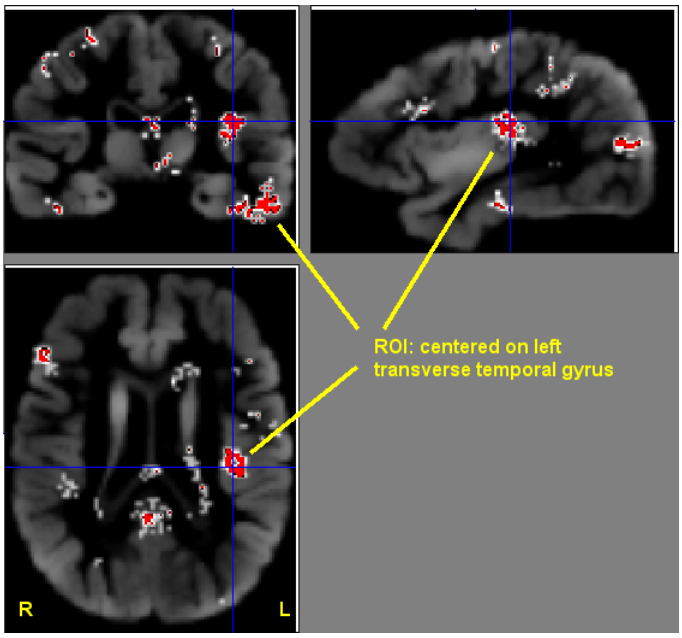

(a) A GM ROI centered on the left transverse temporal gyrus

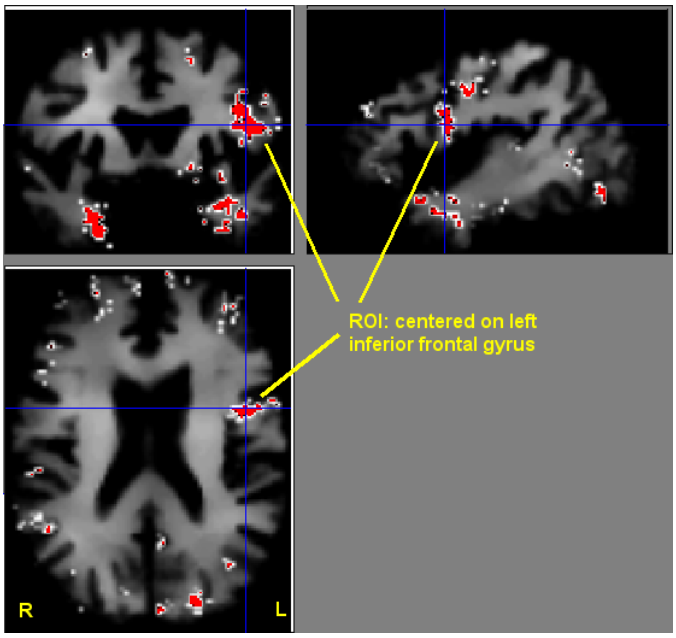

(b) A WM ROI centered on the left inferior frontal gyrus

Fig.4 Additional regions (red) detected in the first association cluster in GM and WM

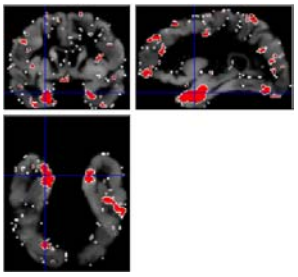

(a) VBM result corresponding to Fig.2 (a)

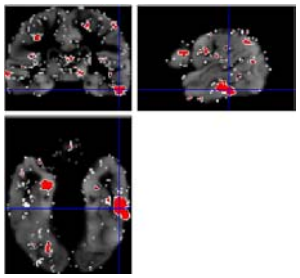

(b) VBM result corresponding to Fig.2 (b)

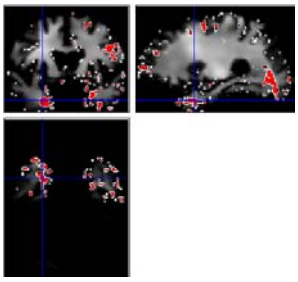

(a) VBM result corresponding to Fig.3 (a)

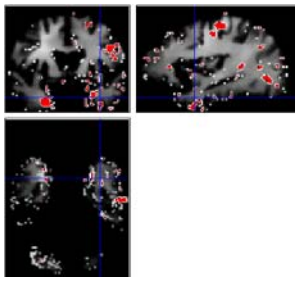

(b) VBM result corresponding to Fig.3 (b)

Figs.5 and 6 VBM analysis results (from SPM99) corresponding to Figs.2 and 3. The *p*-value threshold is 0.05. The ROIs are marked in red.

We also considered the effect of different sizes of the smoothing kernel on registration error and on ROI detection. Table 3 shows the overlap ratio of the largest ROIs detected with different kernel sizes, relative to the largest ROIs found using the 9mm kernel. A smaller kernel renders the results more

sensitive to registration error; in contrast, larger kernels merge interesting signal with noise, rendering morphometry less sensitive. Our results in Table 3 demonstrate these phenomena: both the 5mm-kernel and the 17mm-kernel have smaller overlap ratios than does the 13mm-kernel. Nevertheless, the largest ROIs appear to belong to the same anatomic region, indicating that BMA is relatively robust to kernel size. (Overlap ratios were smaller for WM than for the GM; a likely reason is that the WM results were noisier.)

Table 3. Overlap of the largest ROIs obtained with different methods (BMA or VBM) and different sizes of the Gaussian smoothing kernel. If the largest ROI generated by BMA using a 9mm kernel is X, and that of another kernel size is Y, then the listed ratio is calculated as the volume of the intersection of X and Y, divided by the volume of X.

Tissue	BMA			VBM
	5mm	13mm	17mm	9mm
GM	26.1%	81.4%	59.7%	79.0%
WM	17.0%	27.2%	23.5%	41.6%

DISCUSSION

The clusters generated by BMA contained voxels that have similar probabilistic associations with the MCI clinical variable; these clusters are located in regions previously shown to be associated with reduced volume in individuals with MCI. The major morphological associations with MCI in our cross-sectional BLSA data are centered on entorhinal cortex, which contains critical connections to the hippocampus. The significance of this finding is twofold: first, in our experiment we confirmed prior findings on the association between entorhinal cortex morphology and MCI (Peterson 2001; Jack 1997, 1999, 2000; Fox 1998; Xu 2000; Bobinski 1998; de Toledo-Morrell 2000); second, we have demonstrated that the BMA framework can be applied to imaging data from large-scale studies, such as the BLSA. Other regions of association included the lateral and inferior aspects of the left temporal

lobe; the left insula; and the left inferior frontal region. Associations for several temporal-lobe regions and inferior frontal cortex are consistent with the involvement of these regions early in the course of Alzheimer's disease (Small 2000; Rapoport 2000). These findings may also suggest other regions that show very early changes in MCI, but they require independent confirmation.

Because BMA is based on BN models of morphology-function associations, it is able to incorporate additional types of variables without changing the algorithm. For example, it would be straightforward to add an age variable to these experiments to investigate potential associations among regions related to MCI, and the ages of subjects (this was not done in this paper because our data set doesn't show such a relationship). In addition, the Bayesian model-selection approach used in this paper allows us to compare hypotheses, since a hypothesis corresponds to a Bayesian-network model (or set of models): we can calculate $p(\mathbf{S}|\mathbf{D})$, i.e. the posterior probability of a model **S** given the data **D**, and select the model (or the corresponding hypothesis) with the larger posterior probability. Along with this approach, the domain knowledge of different models (or hypotheses) can also be incorporated as a prior probability distribution over models.

In contrast to BMA, VBM (Ashburner 2000; Davatzikos 2001) uses standard statistical tests to assess hypotheses regarding morphology-function associations. These statistical tests, e.g. t-test, may have limited utility when higher-order associations are present, because a mechanism to automatically formulate the hypotheses of higher-order associations is not embedded in these conventional tests. BMA examines the first-order association hypotheses in searching the first group of homogenous associations; after determining that there is at least one group of first-order associations, BMA continues to search for more complicated association patterns, until no improvement of the model can be made. Therefore, when first-order associations are dominant in the data, such as the MCI data set used in this paper, BMA and VBM will produce similar results. For data sets manifesting nonlinear higher-order associations, BMA and VBM will generate different ROIs, as in Peng (2001).

This application of BMA did not include confounding variables, however these can be incorporated into the analysis as parents of the clinical variable of interest, and applying BMA to these variables. Confounders will render the outcome variable(s) conditionally independent of the image variables; in addition, variables (e.g., gender, perhaps) that affect the nature of structure-function associations would not result in conditional independence, but would result in different clusters depending on the state(s) of these variables. It is important to note that many of the methods we have described in this paper for categorical variables can be extended to BNs consisting of continuous or a combination of continuous and categorical variables (Geiger 1994).

In contrast to methods such as partial least squares analysis (McIntosh 1996), BMA is based on an analysis of categorical variables; we see this as having both benefits and disadvantages. Depending on the nature of the data, discretization of continuous variables may lead to loss of information; however, it is well known that a nonparametric method, such as the Mann–Whitney test, may have statistical power that, in the worst case, approaches that of its corresponding parametric test (i.e., the t-test). If the variables are categorical, or naturally lend themselves to discretization, a distinct advantage of analyzing categorical variables by modeling them with Bayesian networks is the ability to model all associations, including those among clinical and imaging variables, using a common framework. Furthermore, Bayesian networks can model, and the BMA algorithm can recover, highly nonlinear associations among structure and function variables. Thus, we see these approaches as complementary.

Potential errors in our results come from several different sources. The small number of subjects with MCI probably contributes to the multifocal false-positive ROIs, such as those shown in Fig.4 (b). The small number of subjects with MCI also results in errors in the determination of homogenous associations in BMA, which is implemented based on Monte Carlo approximation (Cheeseman 1995; Chickering 1997).

In addition, limitations in the raw image data and image processing, including tissue classification and registration errors, contribute to errors in subsequent analysis. Although HAMMER (Shen 2001b)

is a highly accurate image-registration technique, registration error still degrades the quality of morphology-function analysis. In addition, z-score thresholding for RAVENS-map discretization may be inaccurate, particularly for variables that don't have a bimodal distribution; we plan to evaluate BMA's performance with a variety of discretization schemes. A common discretization method is based on the Gaussian mixture model (e.g., Roberts 1998); however, many of these approaches do not degrade gracefully as the number of subjects decreases. These limitations in the pre-processing steps, however, would have similar impact on other approaches to structure-function analysis.

CONCLUSION

In this paper we show how a novel Bayesian method for morphology-function analysis can be applied for identification of morphological changes that may be associated with MCI. Analysis of data from the BLSA neuroimaging study confirms previous reports of an association between mesial temporal lobe morphology and MCI, providing evidence of the utility of the BMA algorithm. Additional regions in the inferior and lateral aspects of the left temporal lobe are also found in this study.

ACKNOWLEDGEMENT

This work was supported in part by The Human Brain Project, National Institutes of Health grant R01 AG13743, which is funded by the National Institute of Aging, the National Institute of Mental Health, the National Aeronautics and Space Administration, and the National Cancer Institute. We thank the anonymous reviewers for their comments and suggestions.

REFERENCES

Ashburner, J. and Friston, K.J., 2000, Voxel-based morphometry: the methods, *NeuroImage*, **11**: 805-821.

Bobinski, M., de Leon, M.J., Tarnawski, M., Wegiel, J., Bobinski, M., Reisberg, B., Miller, D.C., and Wisniewski, H.M., 1998, Neuronal and volume loss in CA1 of the hippocampal formation uniquely predicts duration and severity of Alzheimer disease, *Brain Research*, **805**: 267-269.

Buntine, W, 1996, A guide to the literature on learning probabilistic networks from data, *IEEE Transactions on Knowledge And Data Engineering*, **8(2)**: 195-210.

Cheeseman, P., and Stutz, J., 1995, Bayesian classification (Autoclass): theory and results, In Fayyad, U., Piatesky-Shapiro, G., Smyth, P., & Uthurusamy, R. (Eds.), *Advances In Knowledge Discovery And Data Mining*, Menlo Park, CA: AAAI Press: 153-180.

Chickering, D.M., and Heckerman, D., 1997, Efficient approximations for the marginal likelihood of Bayesian networks with hidden variables, *Machine Learning*, **29**: 181-212.

Cooper, G., and Herskovits, E., 1992, A Bayesian method for the induction of probabilistic networks from data, *Machine Learning*, **9**: 309-347.

Daly, E., Zaitchck, D., Copeland, M., Schmahmann, J., Gunther, J., and Albert, M., 2000, Predicting conversion to Alzhermer's disease using standardized clinical information, *Archives of Neurology*, **57**: 675-680.

Davatzikos, C., Vaillant, M., Resnick, S., Prince, J.L., Letovsky, S., and Bryan, R.N., 1996a, A computerized method for morphological analysis of the corpus callosum, *Journal of Computer Assisted Tomography*, **20**: 88-97.

Davatzikos, C., 1996b, Spatial normalization of 3D brain images using deformable models, *Journal of Computer Assisted Tomography*, **20(4)**: 656-665.

Davatzikos, C, 1997, Spatial transformation and registration of brain images using deformable models, *Computer Vision and Image Understanding*, **66(2)**: 207-222.

Davatzikos, C., 1998, Mapping of image data to stereotaxic spaces: applications to brain mapping, *Human Brain Mapping*, **6**: 334-338.

Davatzikos, C., Genc, A., Xu, D.R., and Resnick, R.M., 2001, Voxel-based morphometry using RAVENS maps: methods and validation using simulated longitudinal atrophy, *NeuroImage*, **14**: 1361-1369.

Fox, N.C., Warrington, E.K., Seiffer, A.L., Agnew, S.K., and Rossor, M.N., 1998, Presymptomatic cognitive deficits in individuals at risk of familial Alzheimer's disease. a longitudinal prospective study, *Brain*, **121**: 1631-1639.

Friston, K.J., Ashburner, J., Frith, C.D., Poline, J.B., Heather, J.D., and Frackowiak, R.S.J., 1995a, Spatial registration and normalization of images, *Human Brain Mapping*, **2**: 165-189.

Friston, K.J., Holmes, A.P., Worsley, K.J., Poline, J.P., Frith C.D., and Frackowiak, R.S.J., 1995b, Statistical parametric maps in functional imaging: a general linear approach, *Human Brain Mapping*, **2**: 189-210.

Gaser, C., Volz, H.P., Kiebel, S., Riehemann, S., and Sauer, H., 1999, Detecting structural changes in whole brain based on nonlinear deformations-application to schizophrenia research, *NeuroImage*, **10**: 107-113.

Gee, J.C., Reivich, M., and Bajcsy, R., 1993, Elastically Deforming 3D Atlas to Match Anatomical Brain Images, *Journal of Computer Assisted Tomography*, **17**: 225-236.

Geiger, D., and Heckerman, D., 1994, Learning Gaussian Networks, in Proc of *10th Conf on Uncertainty in Artificial Intelligence*: 235-243.

Glymour, C., and Cooper, G.F., (ed.), 1999, *Computation, Causation, and Discovery*, AAAI/MIT Press.

Goldszal, A.F., Davatzikos, C., Pham, D.L., Yan, X.H., Bryan, R.N., and Resnick, S.M, 1998, An image processing system for qualitative and quantitative volumetric analysis of brain images, *Journal of Computer Assisted Tomography*, **22(5)**: 827-837.

Heckerman D, 1997, Bayesian Networks For Data Mining, *Data Mining and Knowledge Discovery*, **1(1)**: 79-119.

Herskovits, E.H., 1991, Computer-based probabilistic-network construction, *Doctoral Dissertation*, Medical Informatics, Stanford University.

Jack, C.R.Jr., Petersen, R.C., Xu, Y.C., Waring, S.C., O'Brien, P.C., Tangalos, E.G., Smith, G.E., Ivnik, R.J., and Kokmen, E., 1997, Medial temporal atrophy on MRI in normal aging and very mild Alzheimer's disease, *Neurology*, **49**: 786-794.

Jack, C.R.Jr., Petersen, R.C., Xu, Y.C., O'Brien, P.C., Smith, G.E., Ivnik, R.J., Boeve, B.F., Waring, S.C., Tangalos, E.G., and Kokmen, E., 1999, Prediction of AD with MRI-based hippocampal volume in mild cognitive impairment, *Neurology*, **52**: pp.1397.

Jack, C.R.Jr., Petersen, R.C., Xu, Y., O'Brien, P.C., Smith, G.E., Ivnik, R.J., Boeve, B.F., Tangalos, E.G., and Kokmen, E., 2000, Rates of hippocampal atrophy correlate with change in clinical status in aging and AD, *Neurology*, **55**: 484-490.

Jensen, F.V., 1996, *An Introduction To Bayesian Networks*, Springer Press.

McIntosh, A.R., Bookstein, F.L., Haxby, J.V., and Grady, C.L., 1996, Spatial pattern analysis of functional brain images using partial least squares, *NeuroImage*, **3**, 143-157.

Morris, J.C., 1993, The Clinical Dementia Rating (CDR): current version and scoring rules, *Neurology*, **43(11)**: 2412-2414.

Morris, J.C., Storandt, M., Miller, J.P., McKeel, D.W., Price, J.L., Rubin, E.H., and Berg, L., 2001, Mild cognitive impairment represents early-stage Alzheimer disease, *Archives of Neurology*, **58**: 397-405.

Peng, H.C., Herskovits, E.H., and Davatzikos, C., 2001, A Bayesian morphological algorithm, submitted to *IEEE Trans. on Medical Imaging*. (http://beast.cbmv.jhu.edu/~phc/papers/tr_bma_2001_1203.pdf)

Peng H.C., Herskovits E, and Davatzikos C, 2002, Bayesian clustering methods for morphological analysis of MR images, in Proc of 2002 *IEEE Int Sym on Medical Imaging: Macro to Nano*: 845-848. (http://beast.cbmv.jhu.edu/~phc/papers/isbi2002_bma_phc.pdf)

Petersen, R.C., Smith, G.E., Waring, S.C., Ivnik, R.J., Tangalos, E., and Kokmen, E., 1999, Mild cognitive impairment: clinical characterization and outcome, *Archives of Neurology*, **56**: 303-308.

Petersen, R.C., Doody, R., Kurz, A., Mohs, R.C., Morris, J.C., Rabins, P.V., Ritchie, K., Rossor, A., Thal, L., and Winblad, B., 2001, Current Concepts in Mild Cognitive Impairment, *Archives of Neurology*, **58**: 1985-1992.

Rapoport, S.I., 2000, Functional brain imaging to identify affected subjects genetically at risk for Alzheimer's disease, *Proc. Natl. Acad. Sci. USA*, **97**: 5696-5698.

Resnick, S.M., Goldszal, A.F., Davatzikos, C., Golski, S., Metter, E.J., Kraut, M., Bryan, R.N., Zonderman, A.B., 2000, One-year age changes in MRI volumes in older adults, *Cerebral Cortex*, **10**: 464-472.

Roberts, S.J., Husmeier, D., Rezek, I., and Penny, W., 1998, Bayesian approaches to Gaussian mixture modeling, *IEEE Trans. PAMI*, **20(11)**: 1133 –1142.

Small, G.W., Ercoli, L.M., Silverman, D.H., et al., 2000, Cerebral metabolic and cognitive decline in persons at genetic risk for Alzheimer's disease, *Proc. Natl. Acad. Sci. USA*, **97(11)**: 6037-6042.

Shen, D.G., Herskovits, E.H., and Davatzikos, 2001a, An adaptive-focus statistical shape model for segmentation and shape modeling of 3D brain images, *IEEE Trans. on Pattern Analysis and Machine Intelligence*, **20(4)**: 257-270.

Shen, D.G., and Davatzikos, C., 2001b, HAMMER: hierarchical attribute matching mechanism for elastic registration, *IEEE Workshop on Mathematical Methods in Biomedical Image (MMBIA 2001)*, Kauai, Hawaii, USA, December 9-10, 2001.

Thompson, P.M., and Toga, A.W., 1996, A surface-based technique for warping three-dimensional images of the brain, *IEEE Transactions on Medical Imaging*, **15**: 402-417.

Thompson, P.M., and Toga, A.W., 1997a, Detection, visualization and animation of abnormal anatomic structure with a deformable probabilistic brain atlas based on random vector field transformations, *Medical Image Analysis*, **1(4)**: 271-294.

Thompson, P.M., MacDonald, D., Mega, M.S., Holmes, C.J., Evans, A.C., and Toga, A.W., 1997b, Detection and mapping of abnormal brain structure with a probabilistic atlas of cortical surfaces, *Journal of Computer Assisted Tomography*, **21**: 567-581.

Tierney, M.C., Szalai, J.P., Snow, W.G., Fisher, R.H., Nores, A., Nadon, G., Dunn, E., and George-Hyslop, P.H., 1996, Prediction of probable Alzheimer's disease in memory-impaired patients: a prospective longitudinal study, *Neurology*, **46**: 661-665.

de Toledo-Morrell, L., Goncharova, L., Dickerson, B., Wilson, R.S., and Bennett, D.A., 2000, From healthy aging to early Alzheimer's disease: in vivo detection of entorhinal cortex atrophy, *Annals of the New York Academy of Sciences*, **911**: 240-253.

Woermann, F.G., Free, S.L., Koepp, M.J., Ashburner, J., and Duncan, J.S., 1999, Voxel-by-voxel comparison of automatically segmented cerebral gray matter – a rater-independent comparison of structural MRI in patients with epilepsy, *NeuroImage*, **10**: 373-384.

Xu, Y., Jack, C.R.Jr., O'Brien, P.C., Kokmen, E., Smith, G.E., Ivnik, R.J., Boeve, B.F., Tangalos, R.G., and Petersen, R.C., 2000, Usefulness of MRI measures of entorhinal cortex versus hippocampus in AD, *Neurology*, **54**: 1760-1767.